Figures of Chapter 2

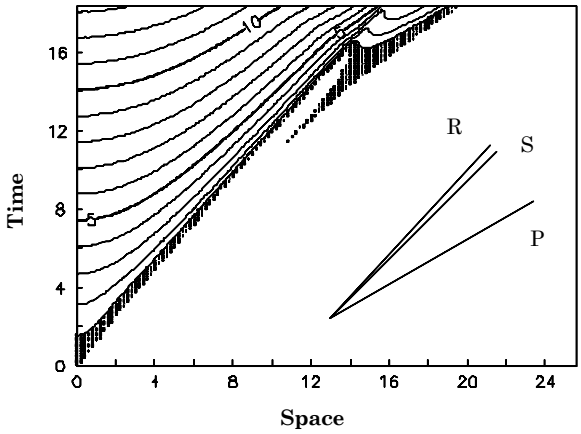

(a)

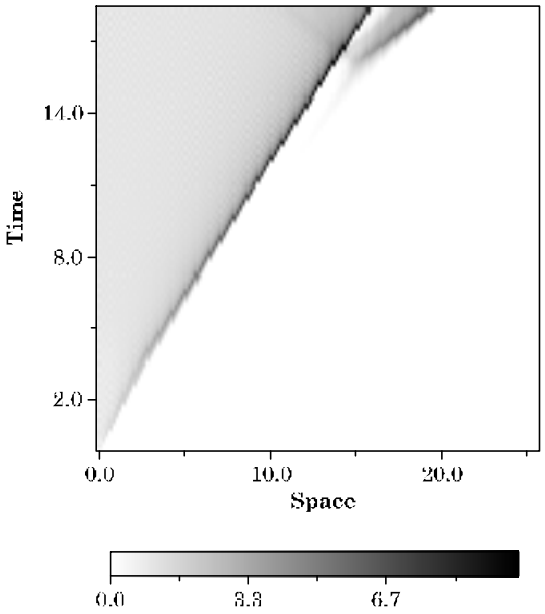

(b)

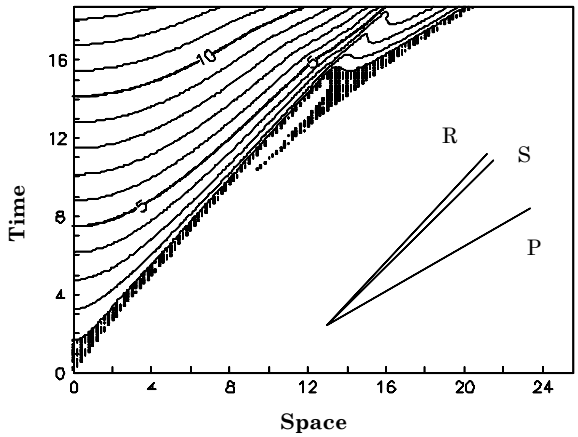

(d)

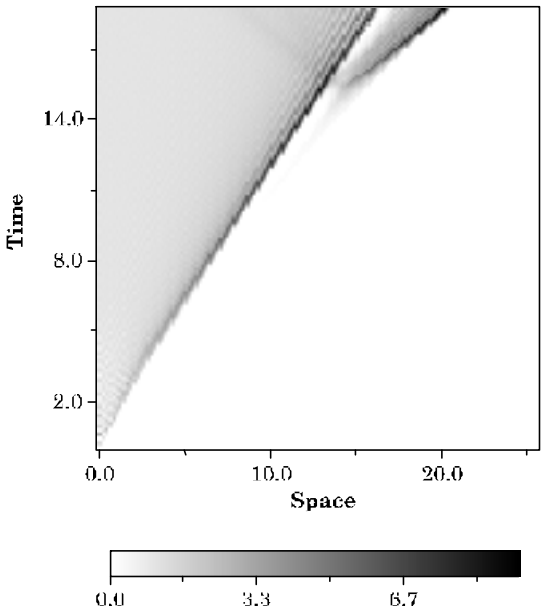

(e)

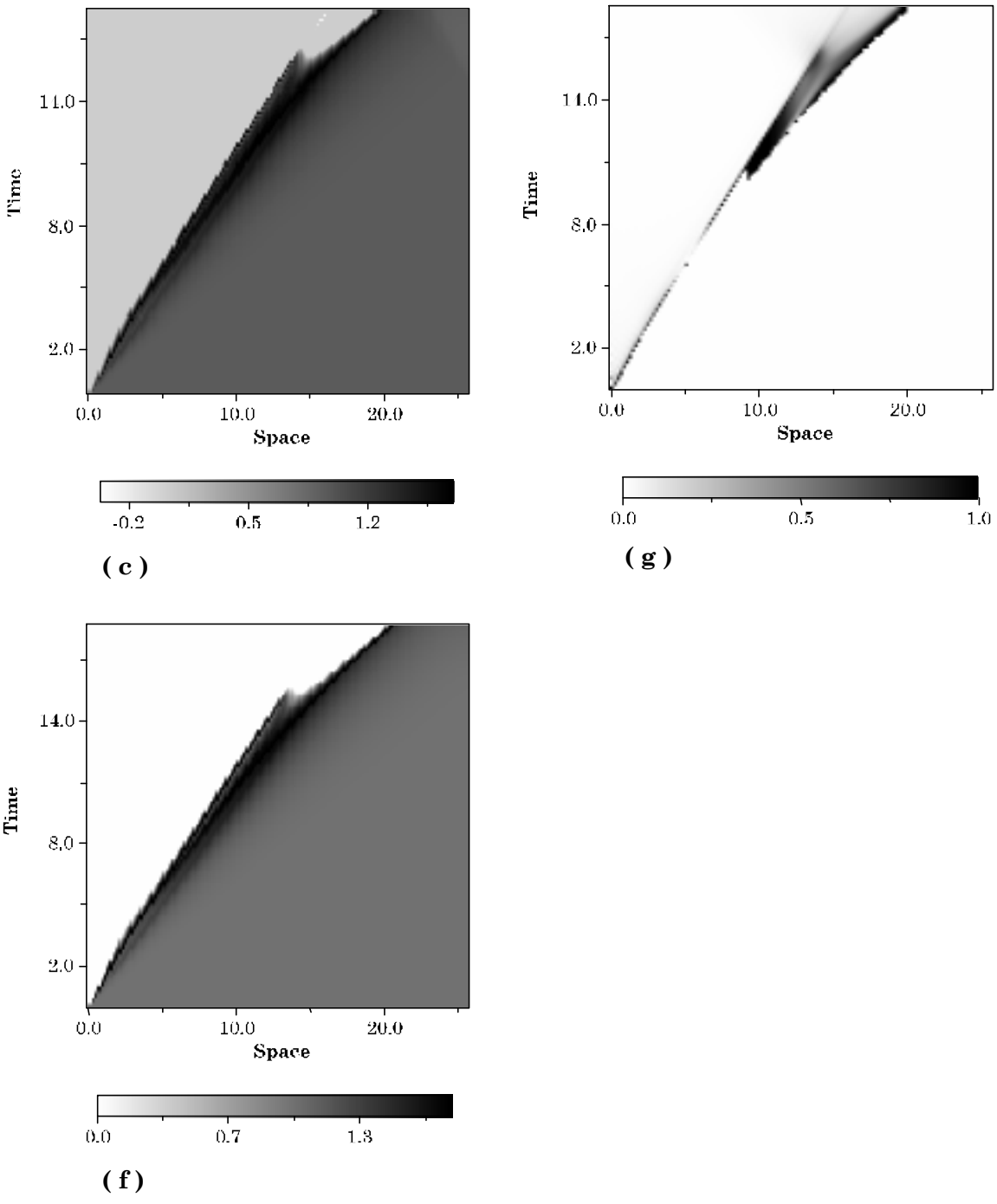

Figure 2.1. Numerical solutions obtained from the BIE (up) and the FD (down) methods for a reference case, in which the strength S is uniform on the fault (S = 0.8, obtained by setting in adimensional units $t_0 = 1$, $t_u = 1.8$ and $t_f = 0$ in the BIE case and $m_0 = 1$, $m_u = 1.8$, $m_f = 0$ and $s_n^{eff} = 1$ in the FD one). In

both methods we fix d_0 = 1.309 and Dx = 0.2 (still in adimensional units). Spatio–temporal evolution of the slip normalized by the characteristic distance d_0 (a) and (d). The slip velocity, (b) and (f), and the total shear traction t (e) and (c). The misfit m between the slip obtained by using the BIE and the FD is shown in (g). The straight lines in the panels (a) and (d) represent the Rayleigh, the S– and the P–wave speeds. See the text for all the details about all the elastic properties of the medium surrounding the fault line and refer to Appendix A for the definition of the misfit function.

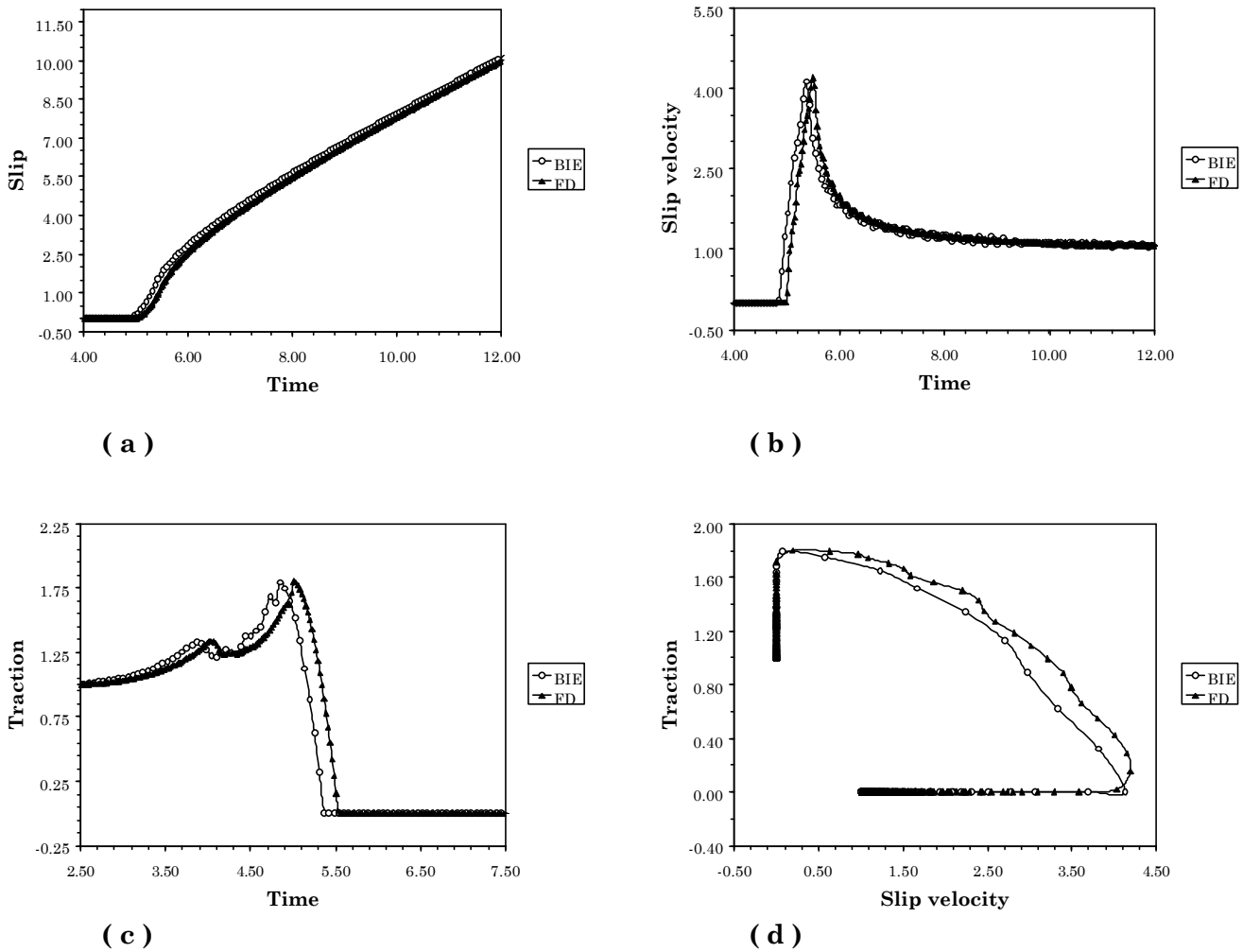

Figure 2.2. Time histories of the slip (a), slip velocity (b), total shear traction (c) and phase diagram (slip rate versus traction) obtained from both

the numerical methods, in the fault point x_1 = 3.9, for the simulation described in Figure 2.1

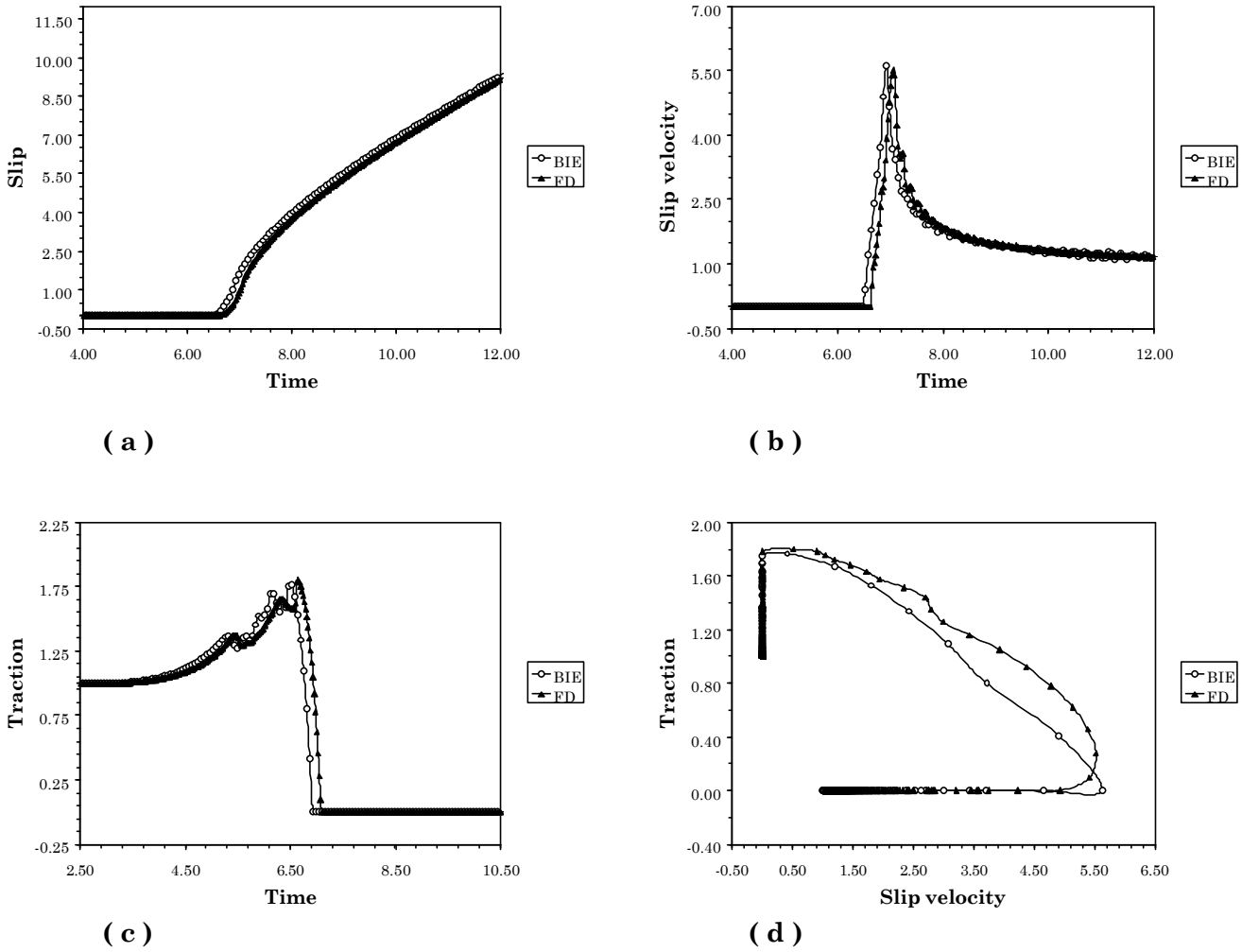

Figure 2.3. The same of Figure 2.2, but in the fault point x_1 = 5.3.

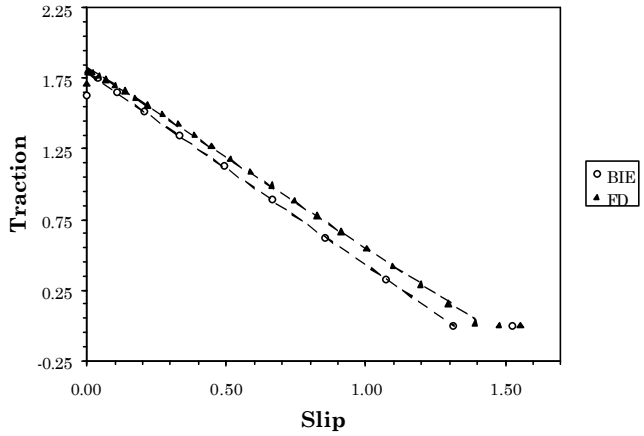

(a)

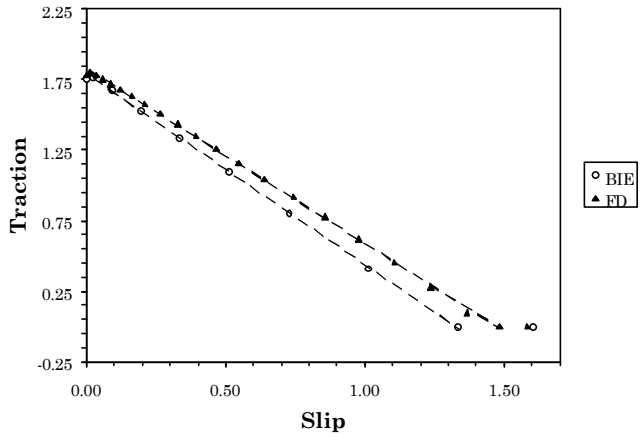

(b)

Figure 2.4. Traction as function of slip as resulting from the two numerical methods (a) in the same fault point of Figure 2.2 and (b) in the point of Figure 2.3. The dashed lines represent the weakening slope.

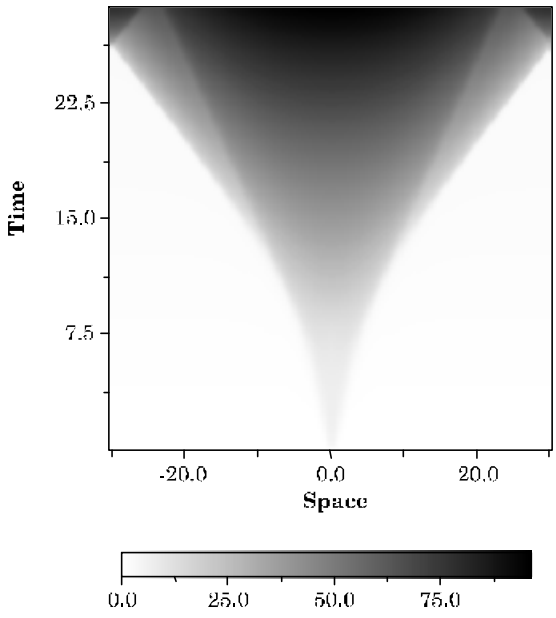
Time
22.5
15.0
7.5
-20.0
0.0
20.0
Space
0.0
25.0
50.0
75.0

(a)

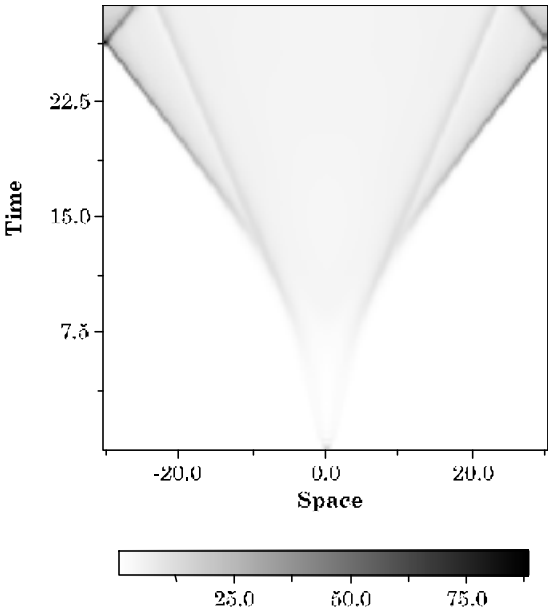
Time
22.5
15.0
7.5
-20.0
0.0
20.0
Space
25.0
50.0
75.0

(b)

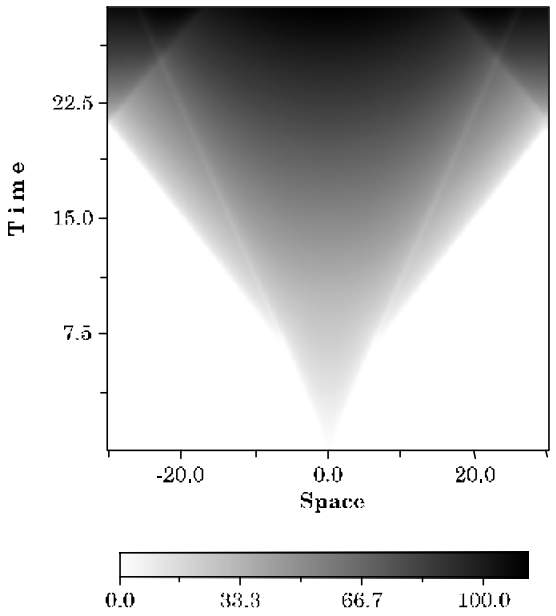
Time
22.5
15.0
7.5
-20.0
0.0
20.0
Space
0.0
33.3
66.7
100.0

(d)

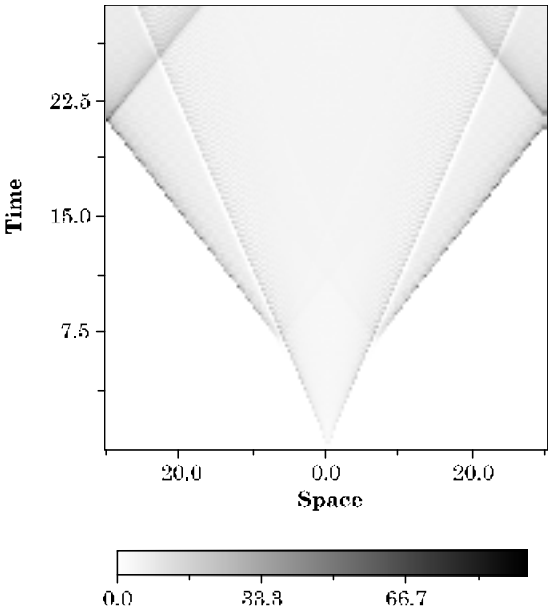
Time
22.5
15.0
7.5
20.0
0.0
20.0
Space
0.0
33.3
66.7

(e)

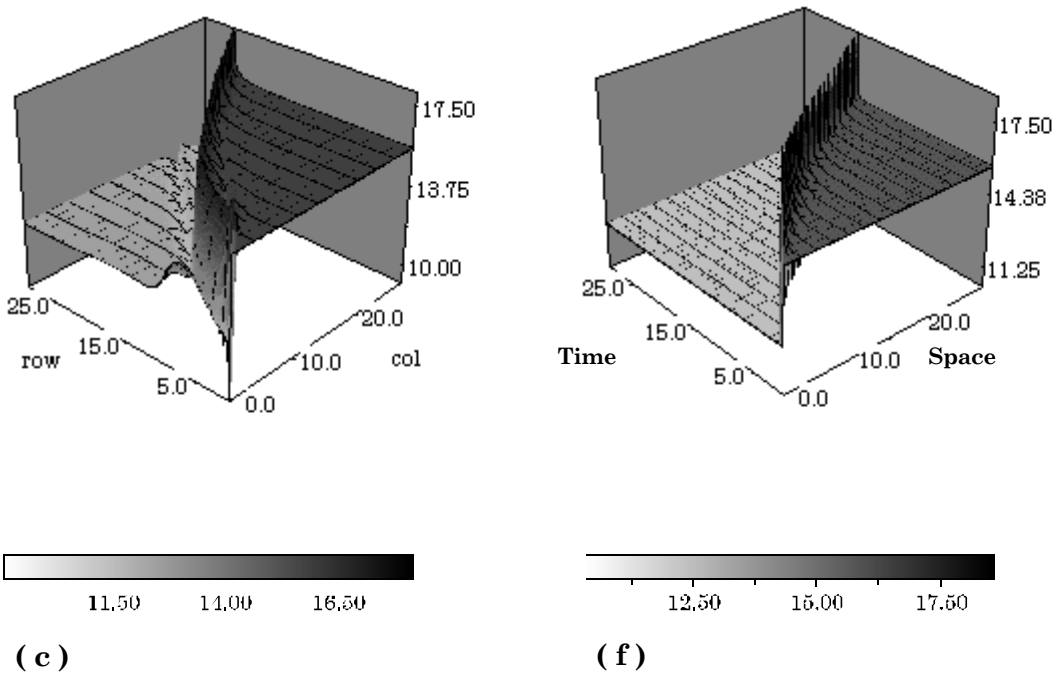

Figure 2.5. (a), (b) and (c) Slip, slip velocity and 3-D view of traction obtained by a FD approach and using the Dieterich–Ruina governing equation. The behavior is very velocity weakening, or strong seismic, and it is characterized by $B - A >> 0$. (d), (e) and (f) Solutions performed by using in the FD a slip–weakening law, with $S < 1.77$. (See Table 1 for details about the constitutive parameters).

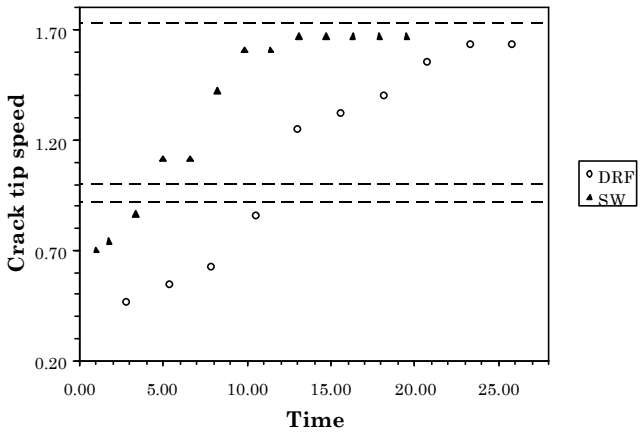

Figure 2.6. Behavior of the crack speed (velocity of the tip) versus time obtained with the Dieterich–Ruina (open circles) and the slip–weakening friction laws (solid triangles). After an initial increase, over v_S the crack speed asymptotically reaches v_P.

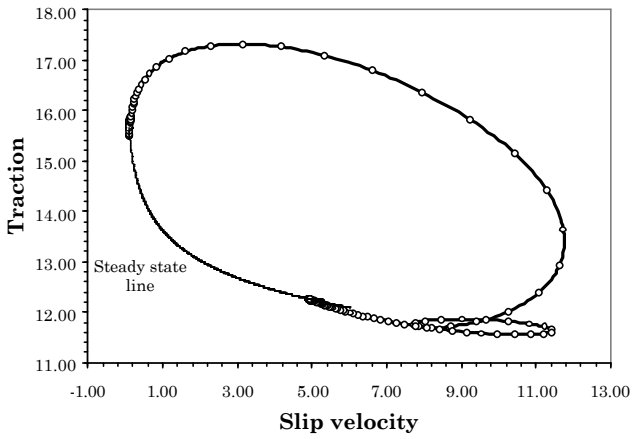

Figure 2.7. Trend of the shear traction as function of slip velocity in the grid point x_1 = 11.8 for the Dieterich–Ruina law. The steady state line plotted in the phase plane emphasizes the fact that the traction is, at the end of the process, in the steady state. The number identifies the different stages of the dynamic rupture: I is the velocity–hardening, II the dynamic acceleration, III the stress release and IV the deceleration.

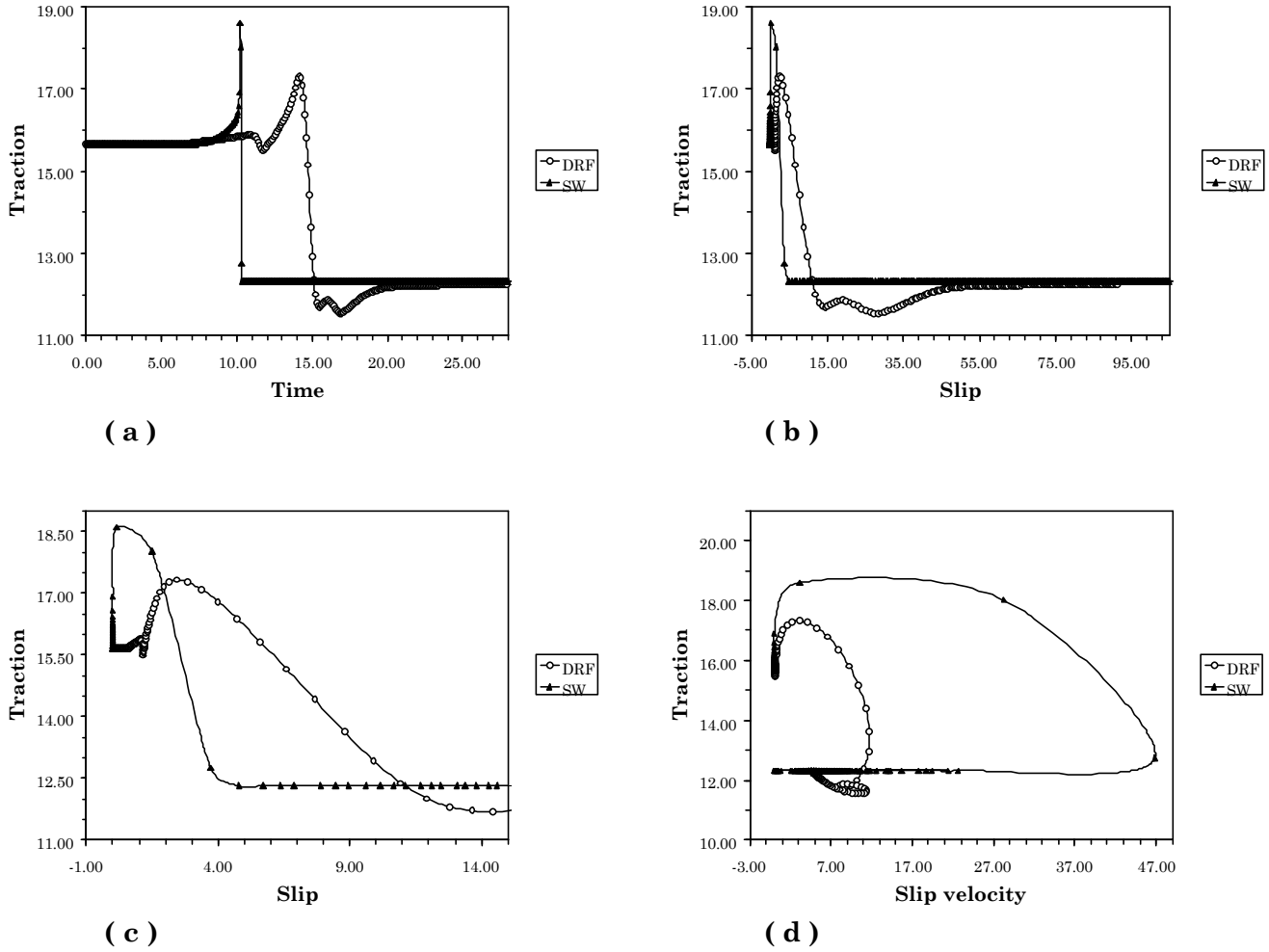

Figure 2.8. Total shear stress (a), traction versus slip (b) and phase diagram (d) in x_1 = 11.8 obtained for the configurations in Figure 2.7 for each governing equation; (c) shows a zoom of the traction behavior as a function of slip during the breakdown process.

Traction vs. Slip

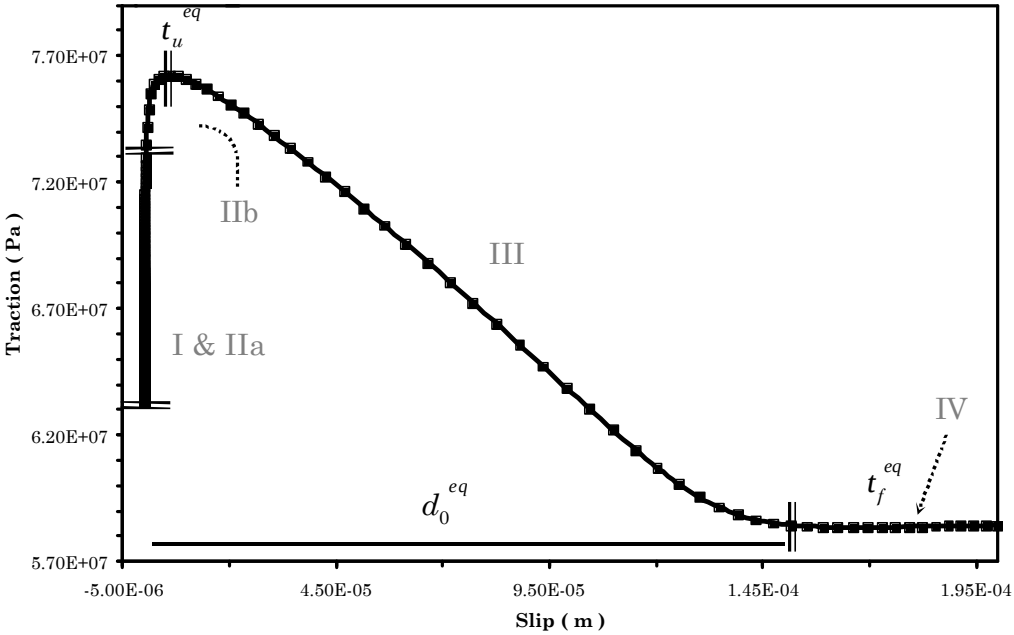

Traction vs. Slip velocity

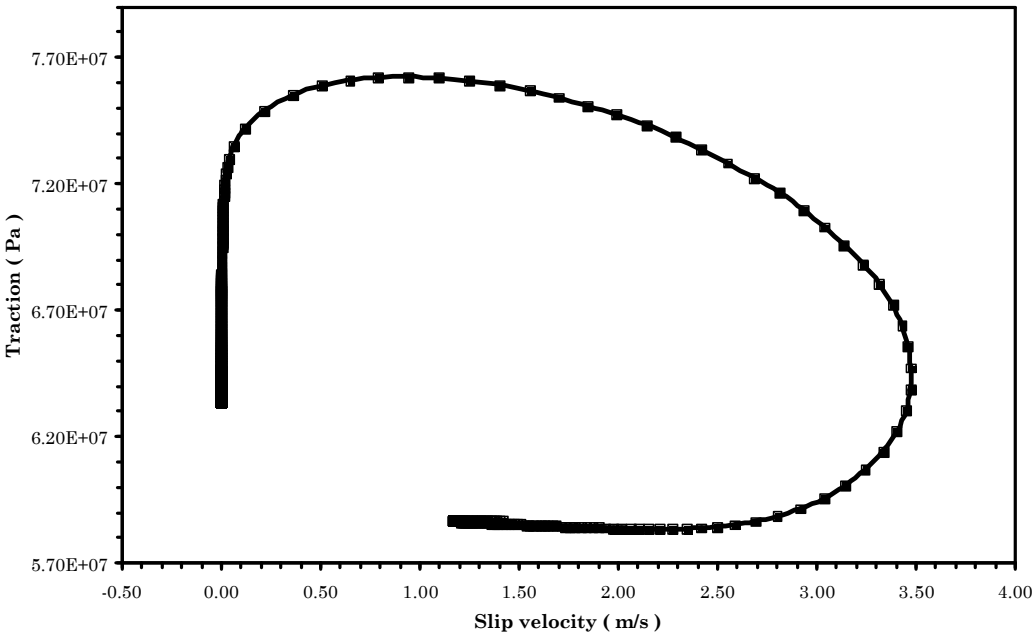

Figure 2.9. Behavior of traction vs. slip (a) and phase diagram (i. e. traction vs. slip rate; b) in the fault point $x_1 = 3.0\ m$ for a propagating rupture obeying to Dieterich–Ruina law. In both the panels we indicate the different stages of the dynamic rupture and the equivalent frictional parameters in the slip–weakening terminology. Initial and constitutive parameters are listed in Table 2.2.

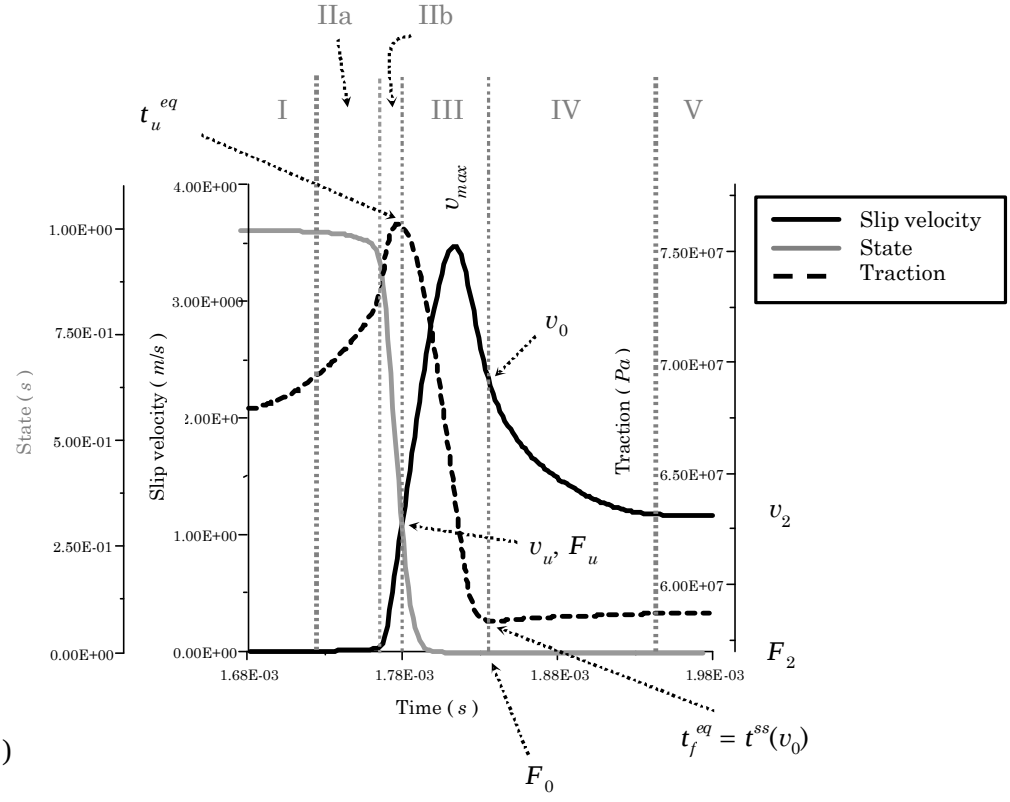

(a)

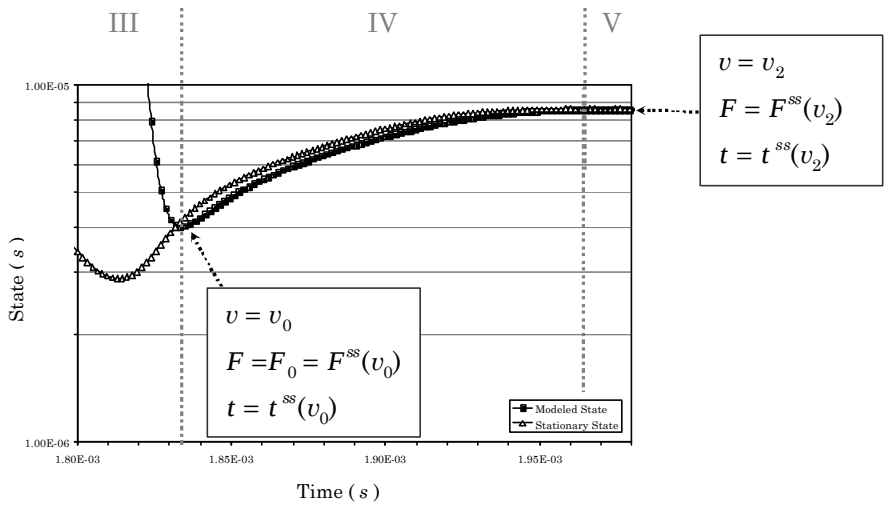

(b)

Figure 2.10. (a) Superposition of the state, slip velocity and traction histories in the same fault point and for the same configuration of Figure 2.9. We indicate all the stages of the dynamic rupture to emphasize that the state evolution controls the increase of slip velocity and fault friction. v_u is the slip velocity value reached when the traction is at its maximum value (t_u^{eq}); v_0 is the value when the fault has slipped of an amount equal to d_0^{eq} and v_2 is the final value of slip rate. (b) Particular of the state variable evolution. We plotted both the numerically modeled state and the steady state curve to emphasize that from the stage the state variable is on its stationary state $F^{ss}(v)$.

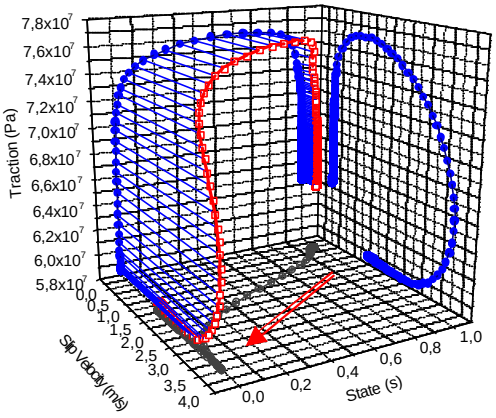
Traction (Pa)
7,8x10^7
7,6x10^7
7,4x10^7
7,2x10^7
7,0x10^7
6,8x10^7
6,6x10^7
6,4x10^7
6,2x10^7
6,0x10^7
5,8x10^7
Slip Velocity (m/s)
0,0
0,5
1,0
1,5
2,0
2,5
3,0
3,5
4,0
State (s)
0,0
0,2
0,4
0,6
0,8
1,0

(a)

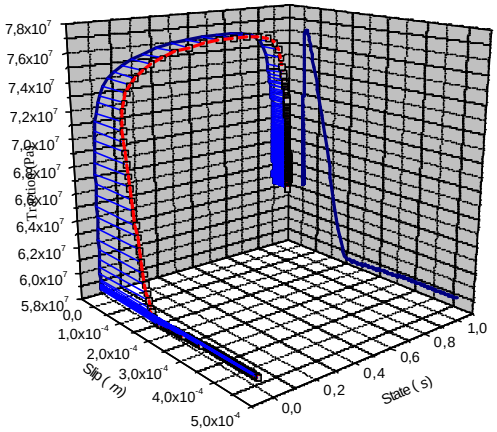
Traction (Pa)
7,8x10^7
7,6x10^7
7,4x10^7
7,2x10^7
7,0x10^7
6,8x10^7
6,6x10^7
6,4x10^7
6,2x10^7
6,0x10^7
5,8x10^7
Slip (m)
0,0
1,0x10^-4
2,0x10^-4
3,0x10^-4
4,0x10^-4
5,0x10^-4
State (s)
0,0
0,2
0,4
0,6
0,8
1,0

(b)

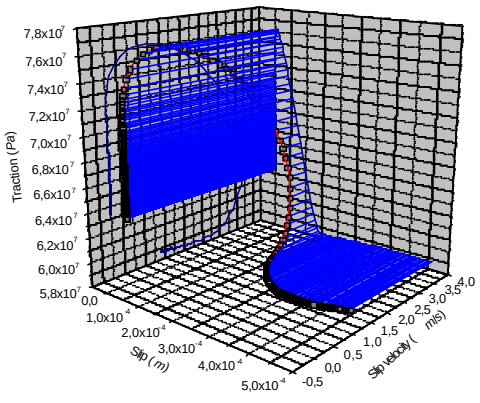
Traction (Pa)
7,8x10^7
7,6x10^7
7,4x10^7
7,2x10^7
7,0x10^7
6,8x10^7
6,6x10^7
6,4x10^7
6,2x10^7
6,0x10^7
5,8x10^7
Slip (m)
0,0
1,0x10^-4
2,0x10^-4
3,0x10^-4
4,0x10^-4
5,0x10^-4
Slip velocity (m/s)
-0,5
0,0
0,5
1,0
1,5
2,0
2,5
3,0
3,5
4,0

(c)

Figure 2.11. 3–D trajectories representing the dependence of fault friction in the same fault point of Figure 2.8 on the slip velocity and state variable (a), on the slip and state (b) and on the slip and slip velocity. The model parameters are the same used in Figure 2.8.

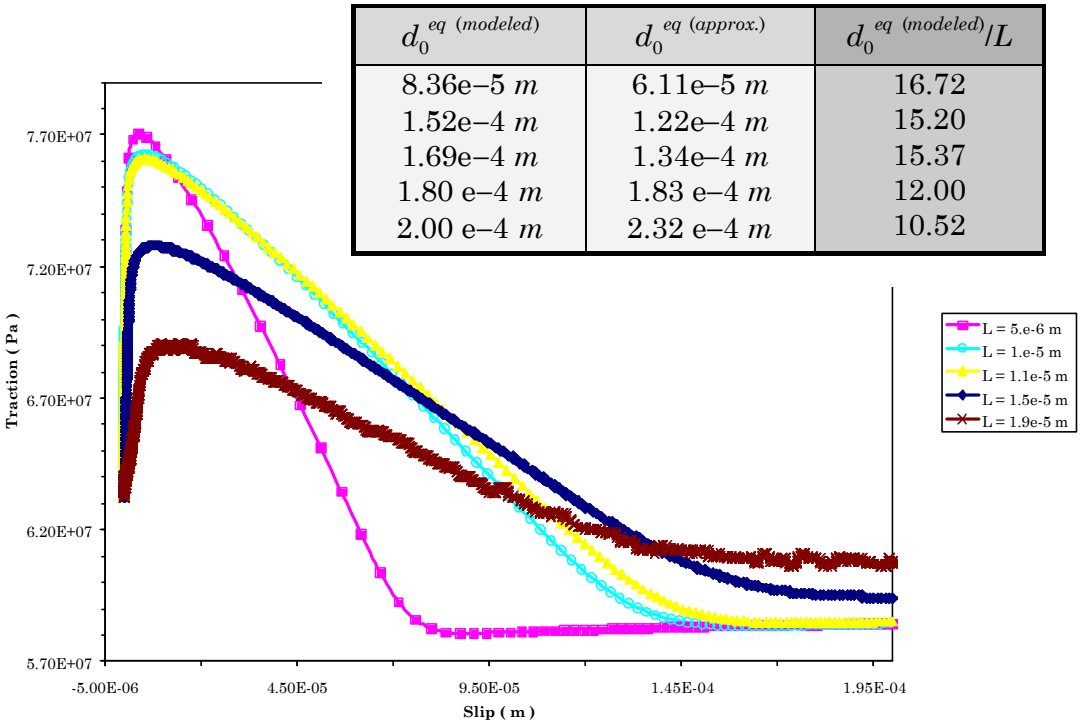

Figure 2.12. SW curve for different characteristic distances L. All the model parameters as the same used before, but we change the spatial discretization in order to correctly resolve dynamics of the configurations with L small (now is $Dx = 0.005\ m$). In the box are showed the modeled and the approximated (by using equation (9) in the text) values of d_0^{eq}.

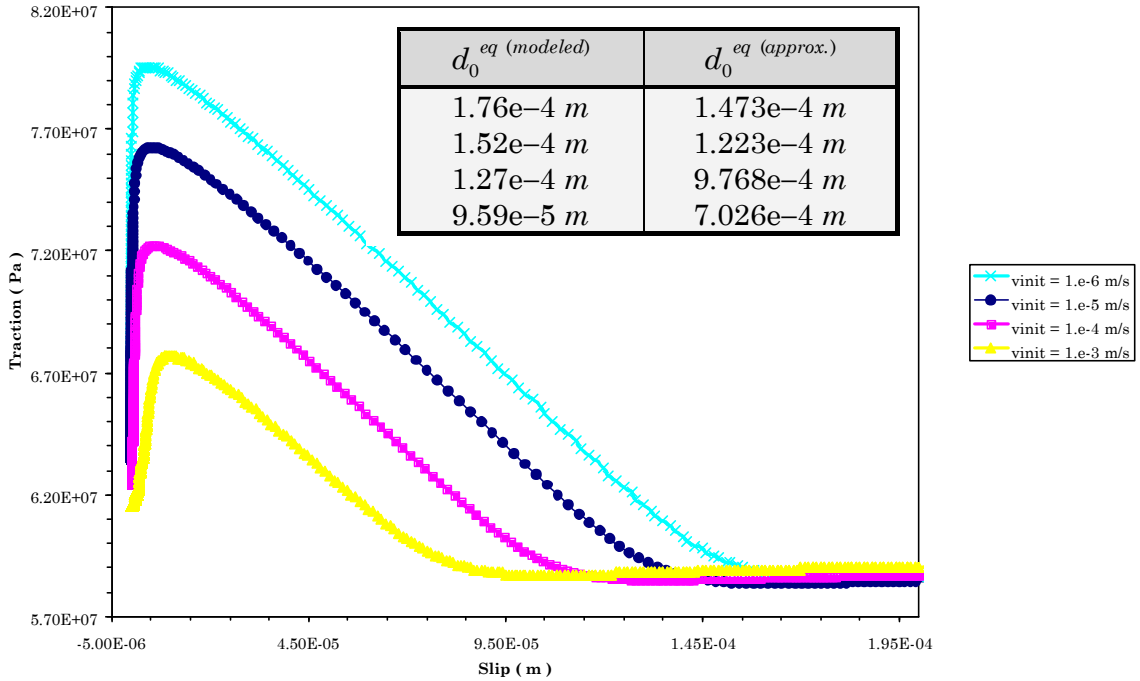

$d_0^{eq\ (modeled)}$	$d_0^{eq\ (approx.)}$
1.76e–4 *m*	1.473e–4 *m*
1.52e–4 *m*	1.223e–4 *m*
1.27e–4 *m*	9.768e–4 *m*
9.59e–5 *m*	7.026e–4 *m*

(a)

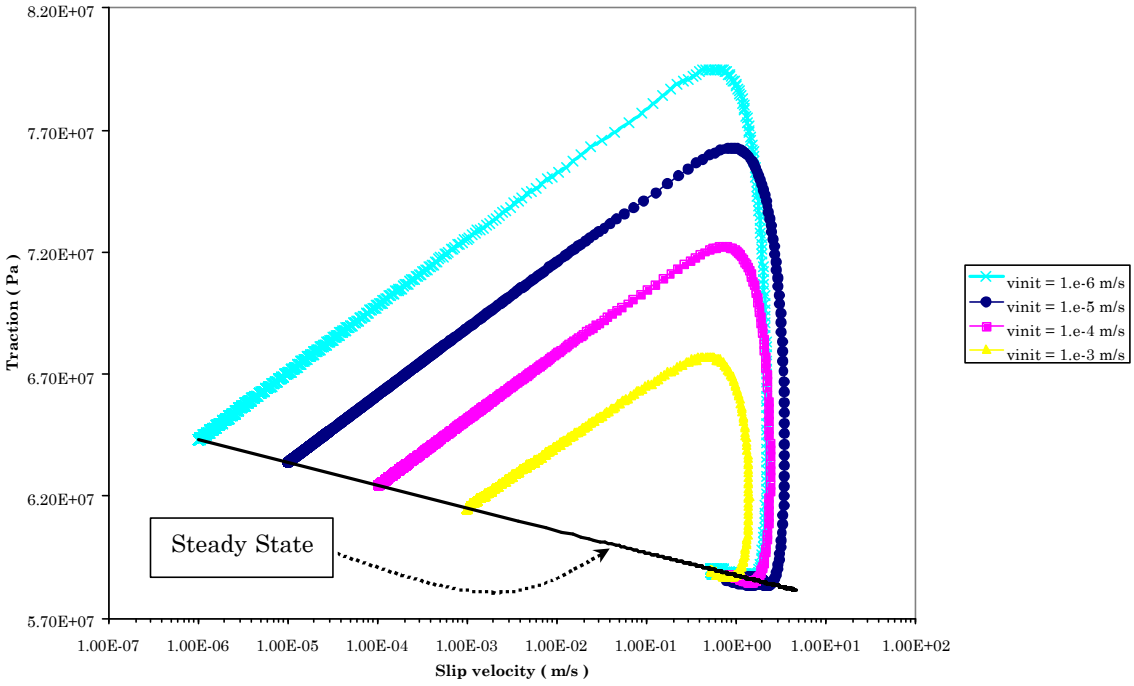

(b)

Figure 2.13. Dependence on the initial slip velocity v_{init}. (a) Traction vs. slip; (b) Traction vs. slip velocity in a logarithmic scale. By varying v_{init} we change also the initial value of the state variable, because it start from its steady state ($F_{init} = L/v_{init}$). We insert in a box in panel (a) the modeled and the inferred values of the equivalent characteristic SW distance d_0^{eq} (approximated values are obtained by using equation (9) in the text). We also plot in (b) the steady state line, in order to emphasize that in all configurations the fault friction in its steady state, but for different v_0 and v_2 values.

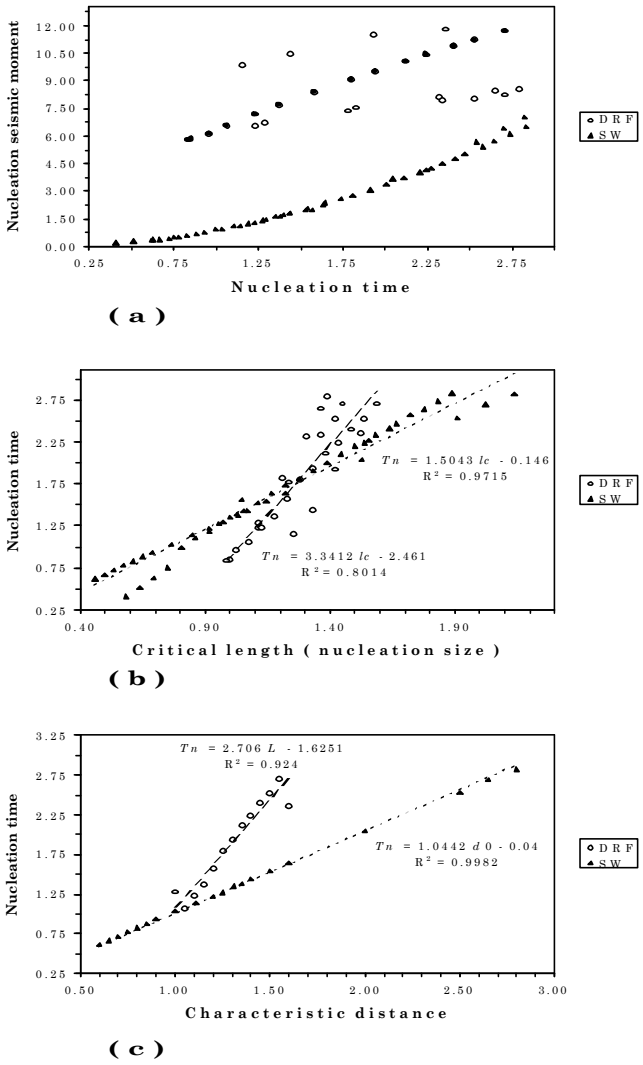

Figure 2.14. Scaling laws between different nucleation parameters inferred by using the slip–weakening and the Dieterich–Ruina constitutive equations derived for homogeneous configurations. For all simulations, performed by the FD method, the convergency–stability conditions (Appendix C) are satisfied. (a) Nucleation seismic moment versus nucleation time; in the DRF case, we represent with dashed circles the configurations with a and b constant (varying only L). The nucleation time versus critical length (b) and versus the characteristic distance (c). For the evaluation of the critical half–length l_c we have choose the parameter h of equation (D.7) as 2/3, according with Dieterich (1992).

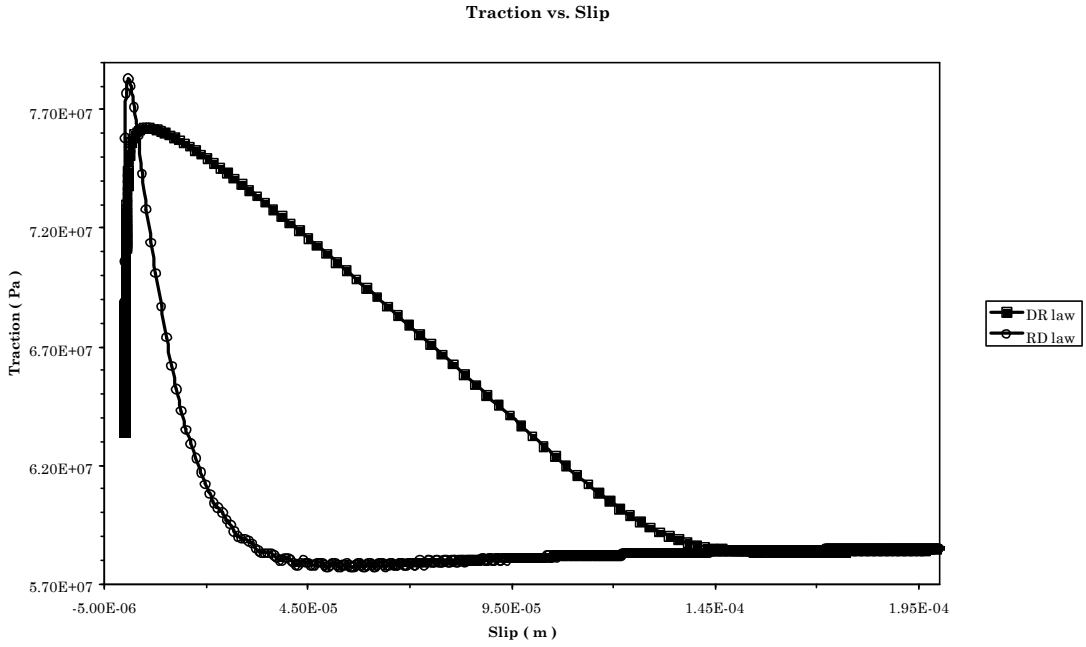

$$\frac{d_0^{\,eq\,(RD)}}{d_0^{\,eq\,(DR)}}$$

Figure 2.15. Comparison between the Dieterich–Ruina (DR, or ageing) law (used in all previous simulations) and the Ruina–Dieterich (RD) law. The analytical expression of friction is identical to equation (3a) (except the + 1 factor in the arguments of the logarithmic terms that do not appear in the RD formulation), but the evolution law is: $(\mathrm{d}/\mathrm{d}t)\ Y = -(v\,Y/L)\ \ln(v\,Y/L)$, instead of (3b).